Plasticity assessment based on Schmid factor in deformed 9Cr-1Mo steel

Manmath Kumar Dash[1, 2], T. Karthikeyan[1], S. Saroja[1*]

[1]*Physical Metallurgy Division, Metallurgy and Materials Group, Indira Gandhi Centre for Atomic Research, Kalpakkam 603102, India*
[2]*Indira Gandhi Centre for Atomic Research, HBNI, Kalpakkam*
[*]*Professor, Homi Bhabha National Institute, Department of Atomic Energy*

[*]Corresponding author: Tel: (+91) 44-27480204; Fax: (+91) 44-27480202; E-mail: saroja@igcar.gov.in

Abstract

Chromium alloyed Ferritic/Martensitic steels are widely used as structural materials in power plants, and considered for core applications of fast and fusion reactors. Characterization and fundamental interpretation of deformed microstructure through crystal plasticity principles are useful for tailoring desired microstructure by optimal processing methods. This study reports the characterization of plastic strain distribution in cold rolled 9Cr-1Mo steel using Electron back scatter diffraction (EBSD) technique. Small orientation changes within the individual grains were studied to gauge the accumulation of 'geometrically necessary' dislocations in deformed material, and correlate with the load geometry. The correlated misorientation angle distribution showed a significant presence of low angle boundaries in the deformed microstructure as compared to the annealed specimen. Crystal orientation map of deformation bands indicated significant intra-grain rotation, and the extent of rotation was distinctly different for different grains. A heterogeneous accumulation of plastic strain distribution is inferred from the grain maps of local misorientation angle (0.5°-5°) and orientation spread parameters. Analysis by Schmid factor criteria (0.4-0.5) showed more than 50% of the grains to exhibit favorable orientation for {110} <111> slip activity, whereas higher stress would be required for plastic deformation of remaining grains. Copyright © 2017 VBRI Press.

Keywords: Polygonal ferrite, EBSD, local misorientation, schmid factor, deformation.

Introduction

The 9Cr-1Mo ferritic steels find use in power plants, and are being considered for wrapper applications of nuclear reactors. They exhibit excellent void swelling resistance as compared to austenitic steels, which is an crucial property for achieving high burn up in fast reactors [**1,2**]. These steels are used in tempered martensite condition that imparts the necessary creep strength at the service temperatures [**3**]. Whereas, manufacturing steps by forming operations are carried out on ferritic polygonal microstructure possessing good ductility. In mechanical forming of components, the plastic strain accumulation is heterogeneously distributed among the individual grains, influenced by variations in shape/size and crystallographic orientations of grains [**4, 5**].

Dislocation motion assisted slip is the common deformation mechanism of metallic polycrystalline materials [**6, 7**]. The dislocation density is increased in the individual grains with increasing amounts of deformation. The 'geometrically necessary' dislocations result in a gradient of orientation within the grain, that can be detected as small shift/rotation of Kikuchi diffraction bands in electron backscatter diffraction (EBSD) experiment [**8,10,11**]. Also, dislocation defects lead to diffused diffraction patterns, but the band contrast quality parameter is not suited for quantitative analysis [**12**]. The parameters such as local misorientation [**13**] and kernel average misorientation (KAM) [**9**] are generally used to correlate the extent of deformation [**14-16**], and assess slip activity due to applied load [**17**].

In deformation, the nature of load geometry, temperature, strain and strain rate dictates the evolution of macro and microtexture of the materials. Deformation modeling covers several length scales, and grain plasticity is an important domain for investigation of deformation

Table 1. Chemical composition (wt %) of the 9Cr-1Mo steel used in the study.

C	Si	Mn	S	P	Cu	Ni	Cr	Mo	N	Fe
0.10	0.75	0.63	0.001	0.02	1.00	1.12	9.27	1.05	0.019	Bal.

texture [**18, 19**]. In our earlier work, the grain boundary character distribution in annealed polygonal grains of 9Cr-1Mo steel has been characterized by EBSD technique [**3**]. The objective of the present study is to assess the effect of cold work on the spatial distribution of grain orientations. The deformation heterogeneity are evaluated based on misorientation angle distribution and microtexture maps such as band contrast, local misorientation angle, KAM and Schmid factor. The study is aimed at interpretation of heterogeneities in deformed microstructures, and assessing the activity of preferred slip system in a forming process.
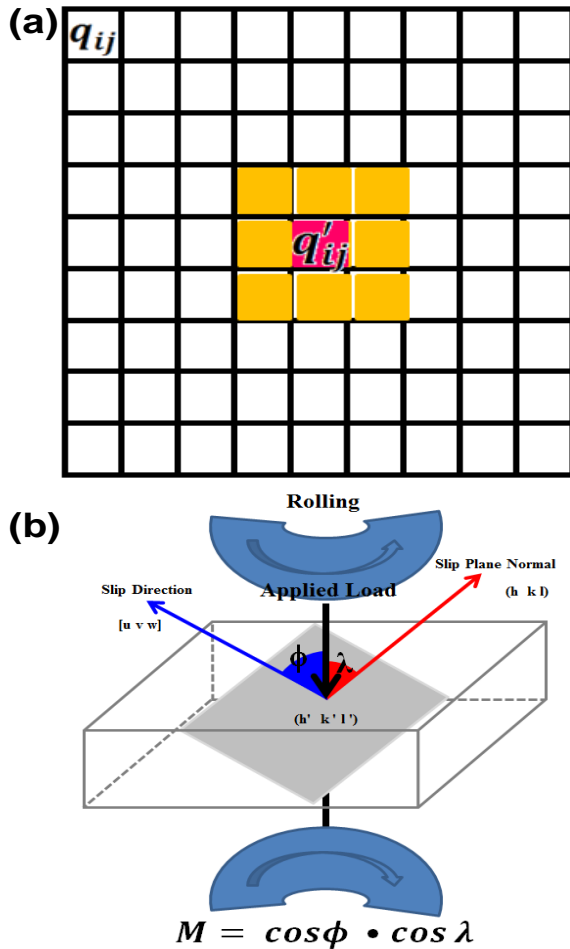

Fig. 1 Schematic representation of (a) local misorientation estimation of each pixel and (b) Schmid factor based calculation for a given slip system.

Experimental

Heat treatment and deformation

The chemical composition of the 9Cr-1Mo (P9 grade) steel used in the present study is given in **Table 1**. The 9Cr-1Mo-0.1C steel samples were solutionized at temperature of 1050^0C for 1 hr, and isothermal annealed (IA) [at 750^0C for 4hr holding time] to effect diffusional transformation of austenite (γ) to ferrite (α) and fine carbide precipitates [**20**]. Lab-scale rolling procedure at

room temperature was used to deform the sample (of initial dimension 20 mm x 10 mm x 5 mm) and reduce the thickness by 20% (to 4 mm) by multiple number of rolling passes.

EBSD characterization

Specimens of the as-heat treated and the subsequent cold rolled steel (at mid-thickness section) were prepared by standard metallographic steps and final electropolishing for microtexture characterization. The EBSD measurements were conducted using W filament FEI XL 30 ESEM - HKL EBSD system. Electropolishing (20% acetic acid + 80% methanol, 10^0C, 15V for 20 second) was found to give a good polished specimen surface suited for EBSD examination. To improve the EBSD signal strength, a high voltage of 30kV and filament current set near to saturation limit settings was utilized. A low SEM magnification (250X) was considered in order to cover adequate number of grains in the specimen, and an EBSD scan step size (0.5µm) was employed. The details of specimen preparation, EBSD scan procedure and optimum experimental settings (detector to sample distance, working distance, and number of detected bands) for unambiguous indexing of diffraction patterns in ferritic steel has been reported previously [21]. The crystal orientation is measured through Euler angle parameters, and the effective angular resolution of misorientation, orientation in EBSD technique is better than 0.5^0[9].

Microtexture data analysis

Local misorientation distribution

The output microtexture scan data was analyzed using HKL Channel-5 software to generate microstructure maps. Small orientation changes across neighboring set of pixels in the EBSD map denote the extent of local deformation. The 'local misorientation angle' parameter was used to estimate the average misorientation angle between a given pixel and its surrounding pixels. Several neighbor domains could be considered for defining the average local misorientation angle [5, 22]. A smaller domain exaggerates errors in orientation measurement, whereas a very large domain could average out the true local variations. In the present study, the filter size of 3x3 pixels was used to produce misorientation maps. **Fig. 1.**(a) shows the schematic of 3x3 grid consisting of pixel point at (i,j) array location and its 8 immediate neighbors; the crystal orientation data qij is compared with its neighbors to find out the misorientations q′ij and the average of the 8 misorientation angles gives the 'local misorientation angle'. Misorientations larger than 5° are regarded as grain boundaries. Adjacent pixel misorientations over a value of 5° are neglected in the calculation, so as to exclude the misorientations associated with discrete sub-grain and grain boundaries. The KAM is an alternate parameter for quantifying the misorientation within grains, wherein the reference point for calculating the misorientation is not necessarily the

central pixel of the grid, but is the average/representative of a group of pixels or the grain ensemble. As the 'local misorientation angle' is very high in few regions of the deformed specimen, the KAM of individual grains in the microtexture data was also calculated to identify the deforming set of grains.
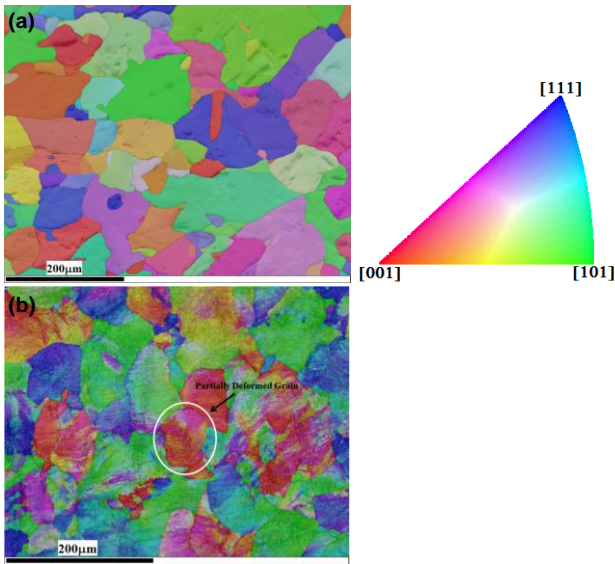

Fig. 2 Overlapped image of Band contrast and Crystal orientation (IPF-Z) map of (a) annealed polygonal ferrite microstructure and (b) deformed microstructure.

Determination of schmid factor

The Schmid factor (M) is an indication parameter which suggests the ease of slip to occur for a particular slip. In a polycrystalline material, M can vary from grain to grain depending on the load geometry and the crystal orientation. In a bcc material, preferred slip direction <uvw> is the close packed <111> direction, while the slip plane {hkl} could be {110}, {112} or {123}. However, in metals, slip appears to be take place predominantly on the slip {hkl} plane of {110} [21]. The M value is calculated for the various possible slip system consitutents of (110) [-1 1 1]/[1 -1 1], (-1 1 0)[1 1 1]/[-1 -1 1], (011)[11-1]/ [1-11], (0-11)[111]/[-111], (101)[-111]/[11-1], (-101)[111]/[1-11] for each orientation data point of deformed specimen using Eq. (1),

$$M = cos\phi \cdot cos\lambda \qquad (1)$$

where, [h'k'l'] is the crystallographic direction aligned with the specimen surface normal that denotes the principal compressive axis of rolling deformation, $cos\phi = \frac{[h'k'l'] \cdot [u\,v\,w\,]}{\sqrt{h'^2+k'^2+l'^2} \cdot \sqrt{u^2+v^2+w^2}}$ and $cos\lambda = \frac{[h'k'l'] \cdot [h\,k\,l]}{\sqrt{h'^2+k'^2+l'^2} \cdot \sqrt{h^2+k^2+l^2}}$. Figure 1(b) shows the schematic configuration of applied load and a slip system for calculation of M [6]. The Schmid factor was calculated using the subroutine of EBSD software by inputting the assumed slip system & load axis, and the

maximum M value among the 12 possible slip system members was calculated and represented as a color map.

Results and discussion

EBSD Map of Annealed and deformed (20% cold rolled) specimen.

Figs. 2(a) and (b) shows the superposed maps of band contrast and IPF-Z in specimens of heat treated and 20% cold rolled steels. In deformed condition, the diffraction patterns tend to be diffused, and thus exhibited poorer band contrast and lower indexing rate (60%), compared to starting annealed sample with 96% indexing. Standard software subroutines were used to assign orientation to unsolved points. The diffusional transformed ferrite produced by isothermal annealing in 9Cr-1Mo steel is comprised of full ferritic structure, while the fine precipitates of carbide phase could not be resolved. A near single orientation of uniform IPF color shade is observed within individual grains of annealed sample. After cold deformation, the slip activity and increased dislocation density deteriorated the Kikuchi diffraction patterns, and indexing rate is reduced. A gradation in color within individual grains observed in crystal orientation color map of deformed specimen is a signature of substructure present in the material [13]. The substructure could be attributed to deformation induced intra-grain rotation [23]. The resulted substructures of dislocation cell in the microstructure showed directional alignment towards the rolling direction. The population of such dislocation cell structure was strikingly dissimilar for different grains, and is also affected by the neighboring grain deformation conditions.
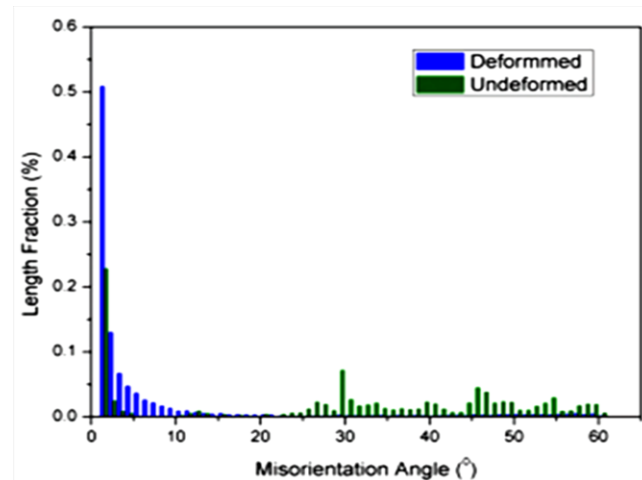

Fig. 3 Comparison of correlated misorientation angle distribution in starting polygonal ferrite microstructure and 20% cold rolled specimen.

Fig. 3. shows the misorientation angle distribution across neighboring pair of pixels, and a higher density of low angle (0.5°–10°) misorientation is revealed in the deformed specimens. Misorientation angle distribution corroborates the observed substructure cells after deformation.
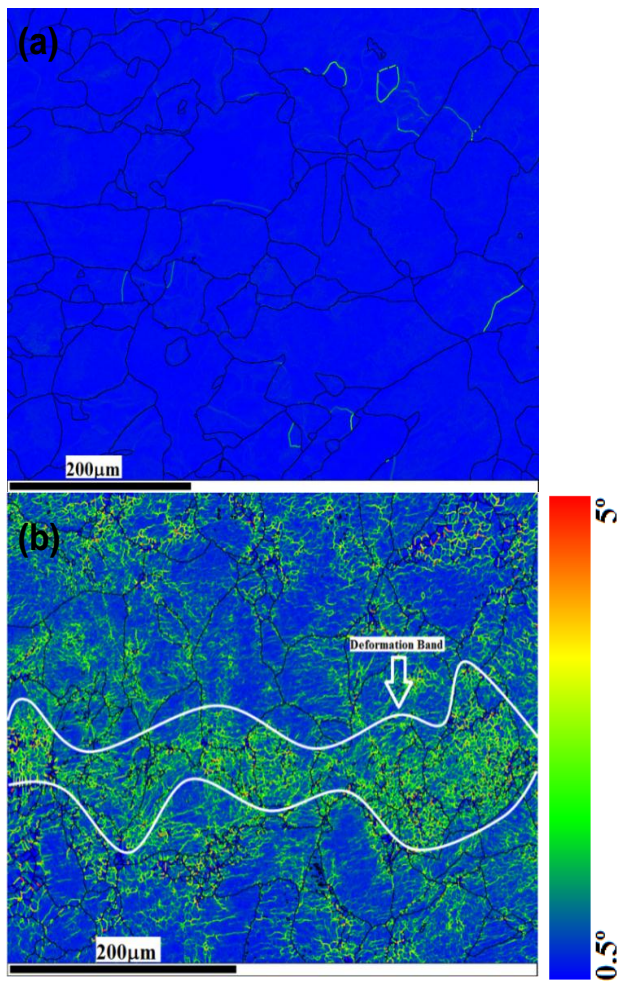
Fig. 4. Superposed maps of the grain boundary (>10° - Black line) and 'local misorientation angle' represented by rainbow colors in (a) polygonal ferrite microstructure, and (b) 20% cold rolled specimen.

Distribution of 'Local Misorientation Angle'

The local misorientation mapping is useful to assess the localization of plastic strain in the microstructure and its relation to overall deformation. It also brings out the extent of intra-granular rotation caused by plastic deformation**. Fig. 4.** (**a**) and (**b**) shows the 'local misorientation angle' map of annealed polygonal ferrite and the 20% cold rolled sample respectively; the color of individual pixel represents the severity of misorientation between 0.5° to 5°. The annealed sample shows a nearly equiaxed grains of ferrite microstructure, and the local misorientation exhibited a uniform low value of 0.5° (close to experimental resolution limit) throughout the grain, irrespective of their shape/size and orientation.

A non-uniform misorientation distribution could be identified in the deformed specimen, which is attributed to the heterogeneous nature of grain deformation. Also, deformation shear band aligned with the rolling direction and covering across number of neighboring ferrite grains could be noticed. One such band marked in **Fig. 4 (b)** is seen to exhibit non-uniform thickness and a wavy morphology.
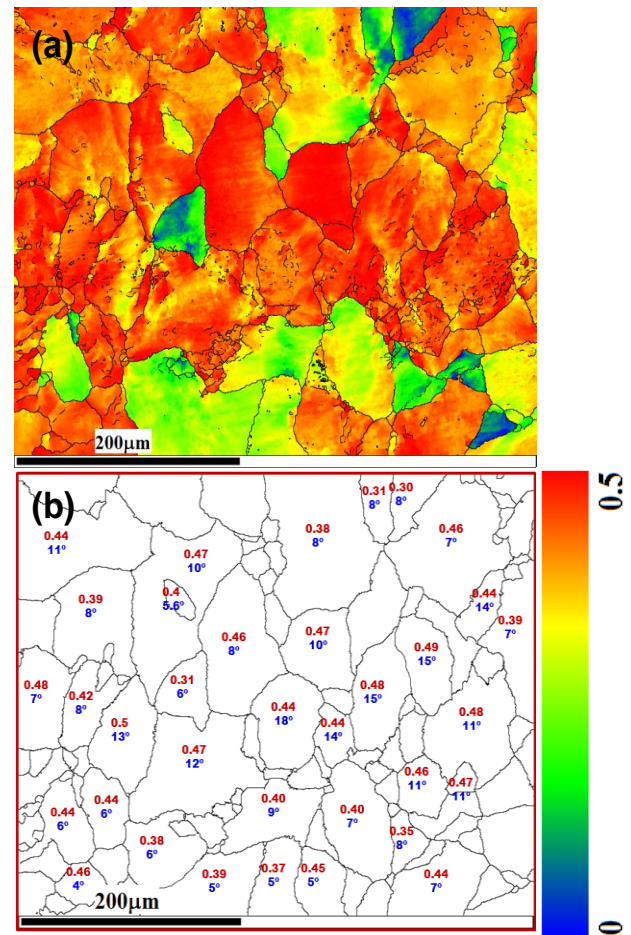

Fig. 5. Maximum Schmid factor of the slip system {110} <111> depicted as a (a) color map, and representation of (b) overall average M, KAM value for individual grains in the cold rolled specimen.

Schmid factor map

The Schmid factor (M) based analysis helps to understand the individual grain deformation and indicates the ease of slip for different grain. In general, Hooke's law applies to the initial elastic deformation stage, associated with elastic stretching of atomic bonds. Whereas, the governing parameter for yielding is the applied load and grain orientation that influences the resolved shear stress, and the dislocation activity on the plausible slip system. The favorable slip system {110} <111> of bcc material has been considered to calculate the individual Schmid values and the maximum value is considered for the analysis. **Fig. 5**(**a**) shows the distribution of maximum M value and the color code indicating the values between 0 and 0.5. The map indicates the ease of slip is favorable for a higher value of M in contrast to the grains with lower M values, which are hard to deform [**24-25**]. The individual grain of the starting annealed sample would possess a single uniform M value. During deformation by slip mechanism, dislocations are accumulated that lead to intra-grain grain rotation and produces substructures with slight variation in orientation. This causes small variations or gradations in Schmid factor even within a single grain. Increase of dislocation density makes the

grains harder (strain hardening), and additional deformation proceeds by activation of slip in other grains with lower M values. The partially deformed grain (Figure 4(b)) could be attributed to deformation activity of adjoining grains along the shear band. All these effects influence the distribution and evolution of plastic strain heterogeneity of a deforming material. The deformation bands (**Fig. 4b**) are found to be wavy character, since the orientation of grains with lower M values restrict the propagation of deformation bands and such band continues spread to over neighboring grains which are easy to deform. **Fig. 5(b)** shows the average Schmid factor and average grain values marked on the individual grains.

The misorientation map is found to be qualitatively useful for understanding the individual grain deformation. As the 'local misorientation angle' map is calculated based on misorientation between neighboring pixels (without any reference to the actual grain domain), it showed a considerably larger scatter within the deforming grain, and only few grains satisfied the expected relation with M value. whereas, the KAM is reasonably homogeneous within the deforming grain in contrast to 'local misorientation angle' [**26-27**].
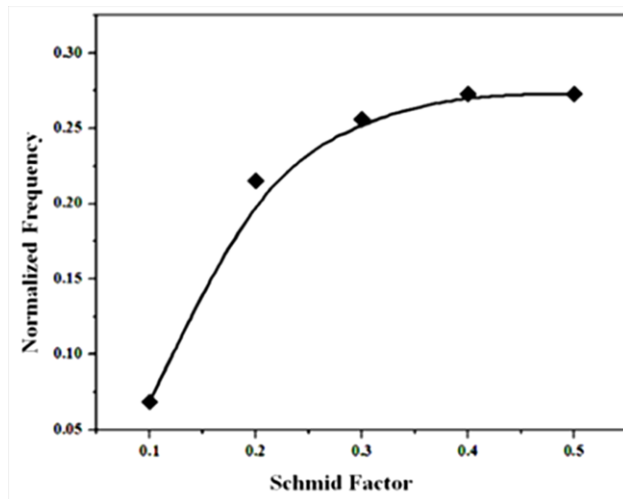

Fig. 6. Normalized frequency distribution of Schmid factor in the cold rolled specimen illustrating the range of M values.

However, a one-to-one relation between M and KAM could not be ascertained from the present microtexture data of deformed ferrite structure. The deformation level could be assessed using the KAM values, and data points with higher KAM value can be considered to be amenably oriented for deformation. **Fig. 6** shows the plot of frequency distribution of Schmid factor values. Principle rolling compressive stresses (along sample thickness direction) and rudimentary slip system had been assumed in the calculations, for the purpose of simplified analysis. About 54% of data points exhibit Schmidt factor (0.4-0.5) favorable for slip activity, whereas the remaining points have lower (<0.4) Schmid factor value, and may require higher external stress for activation of their slip systems. This scatter in M partly explains the considerable

variations of plastic strain observed in deformed microstructures. Further studies on deformation of textured material could confirm this correlation, and could be useful to understand anisotropy of mechanical properties.

Conclusion

The EBSD technique has been used to analyze the plastic strain distribution in a cold rolled 9Cr-1Mo steel with a starting microstructure of polygonal ferrite. The 'local misorientation angle' map is found to replicate the observed extent of deformation qualitatively. Deformation is found to be generally initiated in grains with higher Schmid factor value, but grain deformation is also influenced by the propagating shear bands. Microtexture characterization and analysis presents a useful method for understanding of heterogeneous microstructures of moderately deformed samples.

References

1. Klueh, R. L.; *Int. Mater. Rev.,***2005**, *50*, 287.
    DOI: 10.1179/174328005X41140
2. Klueh, R. L.; Nelson, A. T.; *J. Nucl. Mater.*, **2007**, *317*, 37.
    DOI: 10.1016/j.jnucmat.2007.05.005
3. Karthikeyan, T.; Dash, M. K.; Saroja, S.; and Vijayalakshmi, M.; *Metall. Mater. Trans. A,* **2013***, 44*, 1673.
    DOI: 10.1007/s11661-012-1549-y
4. Musienko, A.; Tatschl, A.; Schmidegg, K.; Kolednik, O.; Pippan, R.; Cailletaud, G.; *Acta Mater.,* **2007***, 55*, 4121.
    DOI: 10.1016/j.actamat.2007.01.053
5. Kamaya, M.; *Mater. Charact.*, **2009**, *60 (2)*, 125.
    DOI: 10.1016/j.matchar.2008.07.010
6. Dieter, G. E.; *Mechanical Metallurgy, McGraw-hill: UK*, **1988**.
7. Hosford, F, *Mechanical behavior of Material, Cambridge university press, US*, **2010**
8. Humphreys, F. J.; J. of Mater. Sci. **2001**, 36, 3833.
    DOI: 10.1023/A:1017973432592
9. Schwartz, A. J.; Kumar, M.; Adams, B. L.; Field D. P.; Electron Backscatter Diffraction in Materials Science (Second ed.), Springer: New York, **2009**.
    DOI: 10.1007/978-0-387-88136-2
10. Winklmann, A.; *Ultramicroscopy*, **2008**, *108*, 1546.
    DOI: 10.1016/j.ultramic.2008.05.002
11. Keller, R. R.; Roshko, A.; Geiss, R. H.; Bertness, K. A., Quinn, T. P., *Microelec. Eng.*, **2004**, *75 (1)*, 96.
    DOI: 10.1016/j.mee.2003.11.010
12. Krieger, N. C. L.; Juul, D. J.; Conradsen, K.; *Mater. Sci. Forum*, **199**4, 157-162, 149.
    DOI: Not Available
13. Field, D. P.; Mater Sci Eng A, **1995**, *190*, 241.
    DOI: Not Available
14. Sutliff, J. A.; *Microsc Microanal*, **1999**, *2*, 236.
    DOI: 10.2320/matertrans.MAW201005
15. Chandrasekaran, D.; Nygårds, M.; *Acta. Mater.*, **2003**, *51*, 5375.
    DOI: 10.1016/S1359-6454(03)00394-X
16. Mino, K.; Imamura, R.; Koiwai, H.; Fukuoka, C.; *Adv. Eng. Mater.*, **2003**, *3*, 922.
    DOI: 10.1016/j.nucengdes.2004.11.006
17. Wagner, F.; Allain-Bonasso, N.; Berbenni, S.; Field D. P.; *Mater. Sci. Forum*, **2011**, *702*, 245.
    DOI: 10.4028/www.scientific.net/MSF.702-703.245

18. Sugiyama, S.; Yanagida, A.; Yanagimoto, J.; *Mater. Sci. Engg.,* **2008**, *478*, 376.
    DOI: 10.1016/j.msea.2007.06.039
19. Parks, D. M.; Ahzi, S.; *J. Mech. Phvs. Solids*, **1990**, *38*, 701.
20. Pickering, F. B.; *Met Technol,***1980,** *7*, 409.
    DOI: Not Available
21. Karthikeyan, T.; Dash, M. K.; Saroja, S.; Vijayalakshmi, M., *J. of Microscopy*, **2013**, *249*, 26.
    DOI: 10.1111/j.1365-2818.2012.03676.x
22. Kamaya, M.; *Mater. Charact*. **2012**, *66*, 56.
    DOI: 10.1016/j.matchar.2012.02.001
23. Field, D.P.; Trivedi, P. B.; Wright, S. I.; Kumar, M.; *Ultramicroscopy*, **2005**, *103*, 33.
    DOI: 10.1016/j.ultramic.2004.11.016
24. Molinari, A.; Canova, G. R.; Ahzi, S.; *Acta metall.,* **1987**, *35*, 2983.
    DOI: Not Available
25. Mika, D. P.; Dawson, P. R.; *Mater. Sci. Engg. A*, **1998**, *257*, 62.
    DOI: Not Available
26. Kamaya, M.; Wilkinson, A. J.; Titchmarsh, J. M.; *Nucl Eng Des*, **2005**, *235*,713.
    DOI: Not Available
27. Brewer L. N.; Othon, M. A.; Young, L. M.; Angeliu, T. M.; *Microsc. Microanal.*, **2006**, *12*, 85.
    DOI: 10.1017/S1431927606060120